Analytical Insights for the Feasibility of Concurrent Black-Start in Inverter-Dominated Grids

Adolfo Anta
AIT Austrian Institute of Technology
Vienna, Austria
Adolfo.Anta@ait.ac.at

Diego.Cifelli
AIT Austrian Institute of Technology
Vienna, Austria
Diego.Cifelli@ait.ac.at

***Abstract*—The replacement of conventional generators with inverter-based resources challenges traditional black-start procedures. The recently proposed idea of concurrent black-start, where multiple grid-forming inverters ramp up their voltages simultaneously, can achieve transient power sharing and bypass the limited ratings of power converters. This paper generalizes our previous work by developing an analytical framework that characterizes the transient currents arising during such a coordinated soft energization. Closed-form expressions capture the influence of delays, ramp times, and droop coefficients on current overshoot and power sharing. The analysis provides explicit conditions, allowing for adequate parameter choice that ensures the feasibility of this concurrent black-start.**

***Index Terms*—black-start, grid-forming, grid restoration**

I. Introduction

The decommissioning of conventional black-start units requires inverter-based resources (IBRs) to assume grid restoration functions [1]–[3]. Despite their high flexibility and controllability, inverters generally have low capacity ratings and cannot sustain short-term overloads. Consequently, following the traditional framework of grid restoration, IBRs could energize only a limited portion of the grid, sometimes even insufficient to provide a cranking path for larger generating units located far away. Moreover, this limited capacity may necessitate dividing the grid into numerous small restoration zones, each energized by a separate IBR, thereby increasing overall restoration complexity.

To address this limitation, our previous work in [4] proposed a simultaneous soft energization strategy for the initial stage of the grid restoration process, in which multiple IBRs ramp up their voltage magnitude concurrently to energize the power grid (or portions of it). This coordinated approach combines the individual capacity ratings of each unit, distributing the initial power demand among them. The concept was introduced primarily as a proof of concept, supported by simulations conducted on a limited number of test systems. However, the generality of the results and the dependence of key performance metrics on grid characteristics and control parameters was not systematically analyzed. This paper substantially extends [4] by developing an analytical framework that characterizes the transient currents arising during concurrent black-start. The main contributions of this work are: first, closed-form expressions for the inverter current during concurrent soft energization, explicitly capturing the impact of grid impedance, droop coefficients, voltage setpoints, and ramp profiles; second, analytical treatment of two practically relevant non-idealities (start-up delays and mismatched ramp times) quantifying their effect on current overshoot and transient power sharing; third, explicit design conditions and guidelines for selecting ramp times and droop parameters that guarantee bounded currents and enable effective transient power sharing. Finally, we show how the analytical results extend to larger networks, with a validation on the IEEE 57-bus system.

II. System Modelling and Control assumptions

We consider a balanced three-phase power system comprising two heterogeneous DC/AC converters, each equipped with an LC output filter and interconnected through lines modelled via π-sections. The study focuses on transmission-level networks, where lines are predominantly inductive, with $X/R \approx 5-20$ in many practical cases. We do not consider any load models, as loads are typically disconnected during the first steps of the grid energization. Both converters employ grid-forming control schemes, where for simplicity we assume a droop controller:

$$\dot{\theta}_j = \omega_{\text{ref}} + m_p(p_{\text{ref}_j} - p_j) \tag{1}$$

where θ_j is the internal converter angle of converter j, ω_{ref} the desired nominal frequency, m_p the droop coefficient, p_{ref_j} the reference active power, and p_j the measured power. Moreover, a PI controller regulates the voltage magnitude:

$$\mu_j = k_{P_j}(V_{\text{ref}_j} - |v_j|) + k_{I_j}\int_0^t (V_{\text{ref}_j} - |v_j|)d\tau \tag{2}$$

with μ_j being the modulation signal, V_{ref_j} the voltage reference (typically a ramp), v_j the voltage after the LC filter of the inverter and V_{dc} the dc side voltage. From now on, we denote all electrical variables in a *dq* frame rotating at the steady state frequency ω^*. The output voltage of a converter j is then:

$$v_{\text{inv}_j} = V_{dc}\mu_j \begin{bmatrix} \cos\delta_j \\ \sin\delta_j \end{bmatrix} \tag{3}$$

where $\delta_j := \theta_j - \theta^*$ is the angle relative to a frame rotating at the steady state frequency ω^*, that is, with $\theta^* = \int_0^t \omega^* d\tau$. Hence, the dynamics of the relative angle δ_j are:

$$\dot{\delta}_j = \omega_{\text{ref}} - \omega^* + m_p(p_{\text{ref}} - p_j) \tag{4}$$

979-8-3315-8138-1

In these average models for the DC/AC converters, the DC side is assumed to be fully regulated by a dc-dc converter to ensure a nearly constant voltage at the DC link regardless of the power on the AC side. The dynamics associated to the output filter are represented by:

$$L_j \dot{i}_{\mathrm{inv}_j} = -Z_{R_j} i_{\mathrm{inv}_j} - v_j + v_{\mathrm{inv}_j} \tag{5a}$$

$$C_j \dot{v}_j = -Y_{C_j} v_j + i_{\mathrm{inv}_j} - i_{g_j} \tag{5b}$$

where i_{inv_j} is the current coming out of inverter j before the LC filter, i_{g_j} being the current after the filter flowing into the grid, $Z_{R_j} = R_j I_2 + J w^* L_j$ with R_j, L_j being the resistive and inductive part of the output filter, $J = \begin{bmatrix} 0 & -1 \\ 1 & 0 \end{bmatrix}$ is the rotation by $\pi/2$, and I_2 is the identity matrix of dimension 2. Moreover, $Y_{C_j} = G_j I + J w^* C_j$ is the admittance of the capacitor and conductance of the output filter of inverter j. Line dynamics equations for the grid can be constructed in an analogous manner, using the incidence matrix representing the network (see [5], [6] for details). We also assume the presence of inner loops that guarantee proper tracking of the desired angle and voltage magnitude after the LC filter. Moreover, these inner control loops (fast current and voltage regulators) are designed with substantially higher bandwidth than the outer loops [7]. Current limiting mechanisms are not included in the inverter models, as converters are not expected to operate at their nominal power during black-start. This ensures both a safety margin under restoration uncertainties and the capability to increase output for voltage or frequency support when necessary.

III. The Concurrent Black-Start Concept

We first revisit briefly the concurrent black-start concept introduced in [4]. We consider a simple grid as in Fig. 1, with two converters on each side, connected by a transmission line modelled as a π-section, where R_g and L_g denote the resistive and inductive part of the transmission line, and $\tilde{C}_j$ and $\tilde{G}_j$ represents the joint capacitance and conductance of the output filter from inverter j and from one of the branches of the π-section. In a soft black-start, the voltage magnitude references are given by ramps starting at t_{0_j} going from 0 to $\bar{V}_j$ in T_{ramp} seconds:

$$V_{\mathrm{ref}_j} = \begin{cases} 0 & \text{if } t < t_{0_j}, \\ \bar{V}_j \frac{t - t_{0_j}}{T_{\mathrm{ramp}_j}} & \text{if } t_{0_j} \le t \le t_{0_j} + T_{\mathrm{ramp}_j}, \\ \bar{V}_j & \text{if } t > t_{0_j} + T_{\mathrm{ramp}_j}, \end{cases}$$

Throughout this work we assume that for $t < t_{o_j}$ inverter j is disconnected from the grid. The same parameters as in [4]

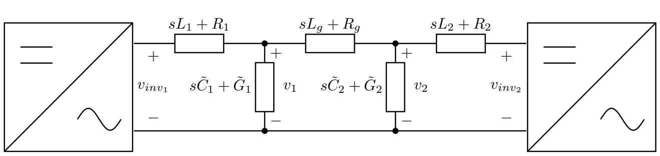

Fig. 1: A line to be energized by two converters on each side.

are used. Fig. 2 compares a black-start scenario with a single inverter and with two inverters, for a normalized ramp time of $T_{\mathrm{ramp}} = 1s$. In the single-inverter case (with the second inverter disconnected), the current exceeds the nominal rating of the unit. For two inverters, equal ramp times and no delay ($t_{0_1} = t_{0_2} = 0s$), both units ramp up simultaneously and remain perfectly synchronized, resulting in the current demand being equally split between inverters and staying well below its nominal value. However, if one inverter initiates its ramp with even a slight delay (arising from communication issues or differences in inverter dynamics) substantial power exchanges may occur between the units: a delay of merely 7ms leads to a pronounced overshoot. This negates the intended purpose of concurrent ramp-up, which is to facilitate proper power sharing during transients.

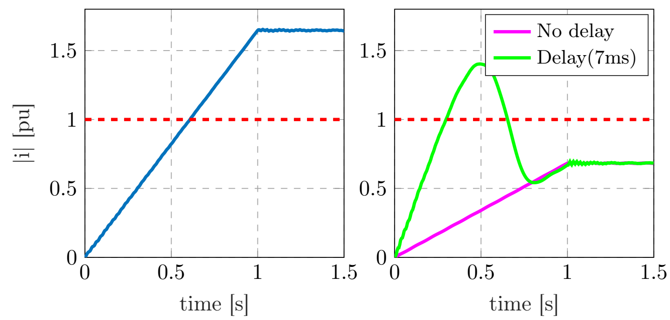

Fig. 2: Energization of a transmission line using one converter (left) and two converters (right), with and without delay.

In the next two sections we present a mathematical analysis of the effects of ramp duration and delays, and derive parameter choices minimizing the overshoot and thus the maximum current for both inverters, that is, $\min \max_t |i_{\mathrm{inv}_j}(t)|$. We first analyse the simplified two-converter system illustrated in Fig. 1 in Sections IV and V, and in Section VI we generalize this framework to arbitrary network topologies.

IV. The impact of start-up delays

We first consider the setup in Section III, with different starting times $t_{0_1} \neq t_{0_2}$, either due to communication delays or different inverter start-up time, and equal ramping times $T_{\mathrm{ramp}_1} = T_{\mathrm{ramp}_2}$. In general, overshoot happens while both units are ramping up, neither right at the starting time nor once the steady state has been reached (see Fig. 2 and Remark 1 below). Hence we focus our analysis to the ramp-up regime, namely the time range $t \in [\max(t_{0_1}, t_{0_2}), \min(t_{0_1}, t_{0_2}) + T_{\mathrm{ramp}}]$, where both voltage references can be modelled as:

$$V_{\mathrm{ref}_j} = \bar{V}_j \frac{t - t_{0_j}}{T_{\mathrm{ramp}}} \tag{6}$$

For ease of notation and without loss of generality, from now on we assume inverter 2 to be delayed, and $t_{0_1} = 0$. Notice that a delay implies that at t_{0_2} the voltage magnitude of inverter 2 is 0, and its phase is zero ($\theta_2(t_{0_2}) = 0$). The reference power at the beginning of a black-start scenario is typically set to 0, as the loads have been disconnected. For $t \in [0, t_{0_2}]$, the phase of inverter 1 evolves according to (1) but with $p \approx 0$ (assuming a nearly lossless grid), hence:

$$\theta_1(t_{0_2}) = \omega_{\mathrm{ref}} t_{0_2}, \quad \theta_2(t_{0_2}) = 0 \tag{7}$$

979-8-3315-8138-1

This can be seen as the initial condition for our time range of interest. This difference in phase will cause transient power transfer between inverters until a steady state is reached where both inverters have very similar phases. As in (5), the dynamics of the line linking the two inverters are given by:

$$L_g \dot{i}_g = -Z_g i_g + B^T \begin{bmatrix} v_1 \\ v_2 \end{bmatrix} \tag{8}$$

with $B = (I_2, -I_2)^T$ and $Z_g = R_g I_2 + Jw^* L_g$. Since the line is mainly inductive, the active power exchanged between both units is given by:

$$p_1 \approx \frac{3}{2L_g\omega^*}|v_1||v_2|\sin(\delta_1 - \delta_2).$$

Notice as well that due to the lack of loads, the steady state frequency is very close to the nominal frequency. We assume the PI control enforces proper tracking of the voltage magnitude reference, that is, $|v_j| \approx V_{\text{ref}_j}$. Hence we can reformulate the angle dynamics from (4) as:

$$\dot{\delta}_1 \approx -\frac{3}{2T_{\text{ramp}}^2 L_g \omega^*}\bar{V}_1\bar{V}_2 m_p t(t - t_{0_2})\sin(\delta_1 - \delta_2) \tag{9}$$

and $\dot{\delta}_2 = -\dot{\delta}_1$, since $p_2 = -p_1$ under the no-losses assumption. The speed of convergence of the angle is influenced by the ramp time, the grid impedance and the droop coefficient. This two nonlinear differential equations can be solved analytically by performing a change of coordinates, defining the angle difference and the angle sum as $\phi = \delta_1 - \delta_2$ and $\Delta = \delta_1 + \delta_2$. The corresponding scalar differential equations for ϕ and Δ are separable and therefore can be explicitly solved using the initial condition in (7):

$$\phi(t) = 2\arctan\left(\tan\frac{\omega^* t_{0_2}}{2} e^{-\xi(t^3 - \frac{3}{2}t_{0_2}t^2)}\right) \tag{10}$$

$$\Delta(t) = -\omega^* t_{0_2} + 2(\omega_{\text{ref}} - \omega^*)t \tag{11}$$

with $\xi = \frac{\bar{V}_1\bar{V}_2 m_p}{T_{\text{ramp}}^2 L_g \omega^*}$. The angles of each inverter can be derived using $\delta_1 = 1/2(\Delta + \phi)$ and $\delta_2 = 1/2(\Delta - \phi)$. The variable ξ then denotes the convergence rates of the angle, and determines the influence of the delays on the overshoot, as shown later.

Once the angle evolution is known, we can obtain the evolution of the grid current, considering a quasi-steady state model of the line dynamics, since the dynamics associated with the lines are much faster than the typical duration of the ramp[1] (see for instance [8]). In that case, the current in the grid can be computed as:

$$i_g = \frac{|\bar{V}_1||\bar{V}_2|}{T_{\text{ramp}} L_g \omega^*}\left[\begin{array}{c} t\sin(\delta_1) - (t - t_{0_2})\sin(\delta_2) \\ -t\cos(\delta_1) + (t - t_{0_2})\cos(\delta_2) \end{array}\right] \tag{12}$$

We can proceed similarly with the dynamics related to the capacitances $\tilde{C}_j$, and lengthy computations lead us to the inverter current in (13), where we have used $\alpha = \frac{1}{\omega^* L_g}$ and $\kappa_j = \omega^* \tilde{C}_j$. If we consider the delay to be relatively small compared to the ramping time ($t_{0_2} << T_{\text{ramp}}$) and $\bar{V}_1 = \bar{V}_2 = 1$, the expressions can be simplified to:

$$|i_{\text{inv}_j}| = \frac{t}{T_{\text{ramp}}}\sqrt{\left(\left(\frac{2}{L_g\omega^*}\right)^2 - 4\frac{\tilde{C}_j}{L_g}\right)\sin^2\frac{\phi}{2} + (\tilde{C}_j\omega^*)^2} \tag{14}$$

which are easier to interpret. Under no delay, $\phi = 0$ and thus the inverter current magnitude is just a ramp, given by $\tilde{C}_j\omega^* t/T_{\text{ramp}}$. The overshoot in $|i_{\text{inv}_j}|$ is then caused by the term influenced by ϕ in (14), which can be seen as the *synchronizing* term enforcing convergence on the phase. This overshoot is thus relatively small whenever the units achieve fast synchronization, making ϕ converge to 0 before the ramp reaches its final value; or in grids characterized by large values of L_g, hence reducing the influence of this synchronizing current. That is, given a grid and a maximum expected delay, it is possible to select a ramping time and a droop value that guarantees the absence of overshoots.

Remark 1: Our analytical solutions are representative only during the ramping period, i.e., when overshoot occurs while the ramp is still increasing. In some cases (e.g., very small droop values), synchronization may be very slow and the overshoot would arise only after the ramp has reached its final value. This situation is not of practical interest, since the resulting overshoot would be excessively large in any case.

We now compare our analytical results against the simulated maximum current in the inverters. Fig. 3 compares our analytical expression for the grid current in (12) against the simulated system, for $t_{0_2} = 7$ms. The analytical response closely matches simulations. Using the expression in (13), we can also analyse the expected overshoot as a function of several parameters, for instance, delays, shown in Fig. 4. The results match fairly well; the discrepancies are caused by the non-negligible line resistance value in our example, and the fact that the inner loops do not track perfectly the reference.

This example demonstrates the explanatory power of our formulation. Many other phenomena can be analysed similarly. Given an expected delay between two units, we can identify the combination of ramp times and droop values that guarantee no overshoot. For instance, increasing the droop value 15% ensures an overdamped response for time delays less than $6ms$. Different droop values can be considered for each unit to improve power sharing during the transient.

V. The Impact of Different Ramp Rates

We now consider the case of different ramp times, e.g., $T_{\text{ramp}_2} > T_{\text{ramp}_1}$, with both ramps starting at the same time ($t_{0_1} = t_{0_2} = 0$), and hence $\delta_1(0) = \delta_2(0)$. As before, for our case of interest overshoot happens during the ramp time, so we limit our analysis to the time range $t \in [t_0, t_0 + T_{\text{ramp}_1}]$, where both voltage references can be modelled as:

$$V_{\text{ref}_j} = \bar{V}_j \frac{t}{T_{\text{ramp}_j}} \tag{15}$$

Looking at (4) it can be seen that $\delta_1(0) = \delta_2(0)$ represents a fixed point of the angle dynamics ($\dot{\delta}_1 = \dot{\delta}_2 = 0$), given

[1] Line dynamics are very relevant for stability in our setup composed uniquely of grid-forming devices. However, our focus is on characterizing the transient response and not verifying stability.

$$|i_{inv_1}(t)| = \frac{1}{T_{\text{ramp}}}\sqrt{\left((\alpha-\kappa_1)\,\bar{V}_1 t\right)^2 + \left(\alpha\bar{V}_2(t-t_{0_2})\right)^2 - 2\,\alpha(\alpha-\kappa_1)\,\bar{V}_1\bar{V}_2 t(t-t_{0_2})\cos\big(\phi(t)\big)} \tag{13a}$$

$$|i_{inv_2}(t)| = \frac{1}{T_{\text{ramp}}}\sqrt{\left(\alpha\,\bar{V}_1 t\right)^2 + \left((\alpha-\kappa_2)\bar{V}_2(t-t_{0_2})\right)^2 - 2\,\alpha(\alpha-\kappa_2)\,\bar{V}_1\bar{V}_2 t(t-t_{0_2})\cos\big(\phi(t)\big)} \tag{13b}$$

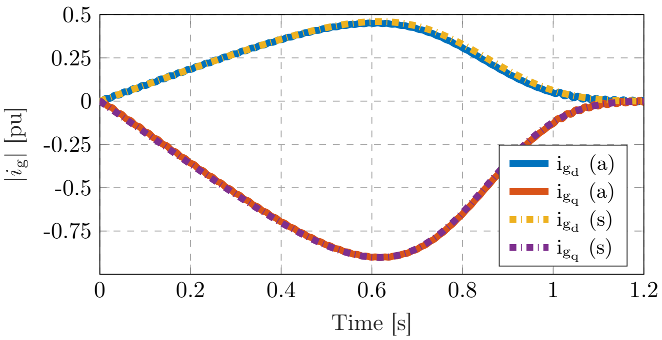

Fig. 3: Grid current in *dq* coordinates, analytical solution (a) and simulation (s), for a delay of $t_{0_2} = 7$ms.

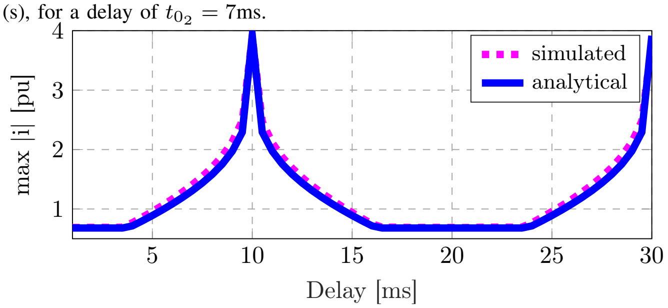

Fig. 4: Current magnitude for inverter 1 as a function of delays.

that the grid is characterized by low losses. As before, the PI control enforces proper tracking of the reference voltage. Given that $\delta_1 = \delta_2$ for our time range of interest, the internal *dq* coordinate frames of each inverter are aligned with the steady state coordinate frame. Hence, both voltages in *dq* coordinates can be represented as $v_j = \left[\frac{\bar{V}_j t}{T_{\text{ramp}_j}}, 0\right]^T$. We can then solve (8) analytically:

$$i_g = \alpha \begin{bmatrix} \cos(\omega^* t) - 1 \\ \sin(\omega^* t) - \omega^* t \end{bmatrix} \tag{16}$$

with $\alpha = \frac{\bar{V}_1 T^{-1}_{\text{ramp}_2} - \bar{V}_2 T^{-1}_{\text{ramp}_1}}{\omega^{*2} L_g}$. For equal voltage references and equal ramp times, i_g is always zero and each inverter just feeds its own capacitor. At the same time, if the setpoints for each unit are different, the ramp times should be adjusted to avoid unnecessary current flows between the two units. We can now construct i_{inv} using (5):

$$i_{\text{inv}_1} \approx \begin{bmatrix} \tilde{C}_1 \bar{V}_1 / T_{\text{ramp}_1} \\ \left(\tilde{C}_1 \omega^* \bar{V}_1 / T_{\text{ramp}_1} + \frac{\bar{V}_1 T^{-1}_{\text{ramp}_1} - \bar{V}_2 T^{-1}_{\text{ramp}_2}}{L_g \omega^*}\right) t \end{bmatrix} \tag{17a}$$

$$i_{\text{inv}_2} \approx \begin{bmatrix} \tilde{C}_2 \bar{V}_2 / T_{\text{ramp}_2} \\ \left(\tilde{C}_2 \omega^* \bar{V}_2 / T_{\text{ramp}_2} - \frac{\bar{V}_1 T^{-1}_{\text{ramp}_1} - \bar{V}_2 T^{-1}_{\text{ramp}_2}}{L_g \omega^*}\right) t \end{bmatrix} \tag{17b}$$

The *d* component is relatively small, so the current magnitude is determined by the *q* component, and is mainly influenced

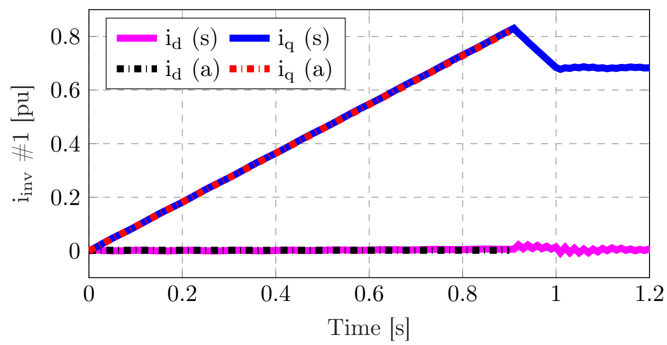

Fig. 5: Current in *dq* coordinates for inverter 1, analytical (a) and numerical solution (s), for $T_{\text{ramp}_1} = 0.9$s and $T_{\text{ramp}_2} = 1$s.

by two components: the capacitor on the side of the inverter, and the exchange of current between inverters. Fig. 5 shows the current evolution for one inverter, with $T_{\text{ramp}_1} = 0.9$s and $T_{\text{ramp}_2} = 1$s. At $t = T_{\text{ramp}_1}$ the current starts ramping down until the steady state is reached at $t = T_{\text{ramp}_2}$. Our analytical expressions are valid only for $t \le T_{\text{ramp}_1}$ and do not model this second ramp, but the overshoot always corresponds to the first ramp. Hence, our formulas in (17) are descriptive for the relevant time interval and allow us to estimate the maximum current. As before, we can simplify the expression for the currents to better interpret them. Assuming $\bar{V}_1 = \bar{V}_2 = 1$p.u and $\tilde{C}_1 = \tilde{C}_2$, a sufficient condition to avoid overshoots is given by:

$$L_g \tilde{C} \omega^{*2} >> \frac{T_{\text{ramp}_2} - T_{\text{ramp}_1}}{T_{\text{ramp}_2}} \tag{18}$$

That is, the relative difference in ramp-up time must be small compared to the line impedance parameters. Many insights can be derived from this set of equations. For grid code requirements, this implies that, for black-start units connected close to each other, the tolerances have to be kept small. Moreover, an inverter exhibiting a slower ramp rate will experience a higher current compared to one with a faster ramp response. Fig. 6 shows the expected maximum currents (computed as the maximum of (17) and the steady state value) against the simulation, for different ramping times. The analytical expression matches well the expected overshoot, with the largest errors observed when there is barely any overshoot, since then the mean peak does not happen during ramp up time but rather due to any minor oscillation occurring right after the ramp has been reached. In any case, those cases are barely relevant as the overshoot is nearly negligible.

Remark 2: For clarity, we have presented the cases of distinct delays and ramp times independently, allowing for a clearer understanding of their respective influences. The combined effect can be described using the approach in

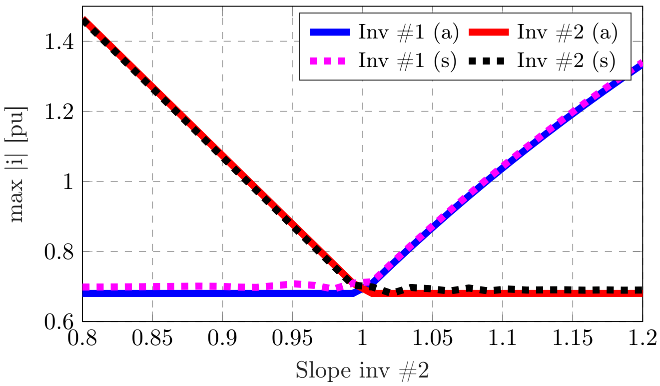

Fig. 6: Overshoot as a function of the second slope ($1/T_{\text{ramp}_2}$), for $T_{\text{ramp}_1} =$ 1s. The numerical simulation is denoted by (s), the analytical results are represented with (a).

Section IV, as the differential equations describing the angle dynamics remain separable under different ramp times.

VI. Extension to large transmission grids

So far we have only considered a simple case with two converters interconnected through a π-section. For more complex grids, an analytical solution for the angle dynamics cannot be directly obtained. To proceed, we perform first a Kron reduction to retain only the converter nodes. Since, as detailed before, line dynamics do not influence the overshoot during the concurrent black-start, a singular-perturbation argument [9] justifies a model reduction step leveraging time-scale separation between the fast line dynamics and the slow ramp behaviour. One may then replace the full high-order reduced transfer function by a single π-section whose series and shunt parameters match the complex admittance of the exact reduced model in a neighbourhood of 50Hz. The complex admittance of the Kron-reduced matrix can be written as:

$$Y_{\text{red}}(j\omega) = \begin{pmatrix} Y_{11}(j\omega) & Y_{12}(j\omega) \\ Y_{21}(j\omega) & Y_{22}(j\omega) \end{pmatrix}.$$

The admittance of a lossy π-section is:

$$Y_{\pi}(j\omega) = \begin{pmatrix} Y_{sh,1}(j\omega) + Y_s(j\omega) & -Y_s(j\omega) \\ -Y_s(j\omega) & Y_{sh,2}(j\omega) + Y_s(j\omega) \end{pmatrix}$$

with the parametrization:

$$Y_s(j\omega) = (R_g I_2 + J\omega L_g)^{-1}, \quad Y_{sh,j}(j\omega) = \tilde{G}_j I_2 + J\omega \tilde{C}_j.$$

Matching both admittances at the nominal frequency ($Y_{\pi}(j\omega^*) = Y_{\text{red}}(j\omega^*)$), the equivalent parameters of the π-section can be easily computed. This two-step approach allows us to apply the previous formulas to more complex grids.

We assess our analytical approach on the IEEE 57-bus system (using the tool in [10]), using the same control parameters as in [4] (in p.u.). Since the original line characteristics yield unrealistic R/X ratios (around 1) for transmission grids, we increase the inductive part of the lines by a factor of 10. We repeat the previous study for different delay values. Fig. 7 shows how the results match fairly well, similar to the case of a single π-section. This verifies that the pattern is similar across different grids, and the derived expressions are accurate as well in large grids. Similar results were obtained for the case of different ramp times, not shown here due to lack of space. Finally, while in this paper the topic in transformer energization has not been considered, [4] has shown that this idea of transient power sharing extends to inrush currents.

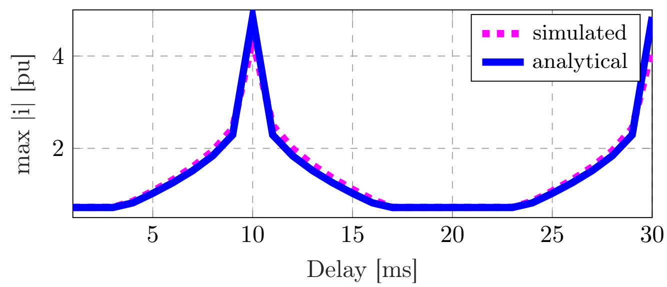

Fig. 7: Current magnitude for one inverter for the 57-bus system.

VII. Conclusions and Future work

This paper has derived closed-form expressions characterizing the evolution of the current magnitude during concurrent black-start, highlighting the dependence on droop coefficients, grid impedance, voltage setpoints and ramp times. Results on the IEEE-57 bus system further demonstrate the generality and validity of the proposed approach. Future work will investigate extensions to networks that are not predominantly inductive (e.g., in distribution grids or lines with series compensation) and explore the potential role of virtual admittance schemes to mitigate overshoot. In addition, we will extend the modelling of inverter behaviour differences beyond delays and ramp-time discrepancies, and validate the concept via Power Hardware-in-the-Loop tests.

References

[1] National Grid, "Demonstration of black start from ders," Technical report [online]. Accessed: 2025/10/14. https://www.nationalgrideso.com/future-energy/projects/distributed-restart, 2021.

[2] A. Alassi, Z. Feng, K. Ahmed, M. Syed, A. Egea-Alvarez, and C. Foote, "Grid-forming vsm control for black-start applications with experimental phil validation," *International Journal of Electrical Power & Energy Systems*, 2023.

[3] J. M. Aniceto, J. Bosch, and A. Anta, "Towards a full automatized ultrafast black start through inverter-based generation," *PowerTech*, 2023.

[4] A. Anta and D. Cifelli, "Analysis of a concurrent soft black start using inverter-based generation," in *IEEE Belgrade PowerTech*, 2025.

[5] T. Jouini and Z. Sun, "Frequency synchronization of a high-order multiconverter system," *IEEE Transactions on Control of Network Systems*, 2021.

[6] F. Dörfler and D. Groß, "Control of low-inertia power systems," *Annual Review of Control, Robotics, and Autonomous Systems*, 2023.

[7] R. Rosso, X. Wang, M. Liserre, X. Lu, and S. Engelken, "Grid-forming converters: Control approaches, grid-synchronization, and future trends—a review," *IEEE Open Journal of Industry Applications*, 2021.

[8] U. Markovic, O. Stanojev, P. Aristidou, E. Vrettos, D. Callaway, and G. Hug, "Understanding small-signal stability of low-inertia systems," *IEEE Transactions on Power Systems*, 2021.

[9] L. Luo and S. V. Dhople, "Spatiotemporal model reduction of inverter-based islanded microgrids," *IEEE Trans. on Energy Conversion*, 2014.

[10] Y. G. Yitong Li, "Simplusgt," https://github.com/Future-Power-Networks/Simplus-Grid-Tool/, 2024.